RSC Advances

ROYAL SOCIETY OF CHEMISTRY

www.rsc.org/advances

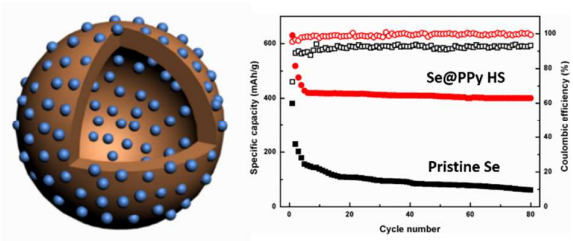

The selenium@polypyrrole hollow sphere composite cathode delivers a reversible specific discharge capacity of 400 mAh/g after 80 cycles at 0.2C.

Journal Name

RSCPublishing

COMMUNICATION

A selenium@polypyrrole hollow sphere cathode for rechargeable lithium batteries

Cite this: DOI: 10.1039/xoxxoooooox

Jing Guo, Zhaoyin Wen*, Guoqiang Ma, Jun Jin, Weiqi Wang, Yu Liu

Received ooth January 2012,
Accepted ooth January 2012

DOI: 10.1039/xoxxoooooox

www.rsc.org/

Selenium@polypyrrole hollow sphere composite cathode delivers a reversible specific discharge capacity of 400 mAh/g after 80 cycles and a 60% reduction in impedance of cycled cells is obtained. The soluble polyselenide species are demonstrated to be confined by PPy hollow spheres, thus inhibiting the shuttle effect to a large extent.

Introduction

Rechargeable lithium batteries have always been attached great importance on account of the rapid progress of portable electronics and electric vehicles as well as the exploitation for wind and solar renewable energy[1]. The desire for rechargeable batteries with high energy density, high efficiency and good safety has been accelerating the development of new energy storage systems [2]. Other than those electrodes or systems based on conventional intercalation chemistry, Li-S [3-6] and Li-O_2 [7-9] batteries which possess incredibly high theoretical energy density and low cost have caught significant attention from relevant researchers currently. However, the cycling performance of Li-O_2 cells is restricted by large polarization and instability of electrolytes [10]. Li-S batteries suffer from shuttle effect, that is, polysulfides, the intermediate discharge products, dissolve in electrolytes and migrate to the lithium anode leading to rather poor cyclability. In addition, the sulfur cathode is both electronic and ionic insulator, which also limits the practical applications of Li-S battery [3]. Therefore, the synthesis of new electrode materials and the study of their performance is indispensable for the development of lithium batteries.

Selenium, belonging to the same group as sulfur, with a high specific theoretical capacity of 675mAh/g or 3253mAh/cm^3 was first demonstrated as a candidate of cathode material for lithium and sodium rechargeable batteries by Abouimrane et al. [11]. They investigated structural mechanisms for Li insertion in selenium-based electrodes and their results show that the trigonal structural Se finally transforms into an antifluorite-type Li_2Se phase during discharge. They also found that the redox shuttle effect in Se cathode was relatively less severe as compared to that in S cathode. Li-Se batteries are supposed to possess a large volumetric energy density that is of greater importance than gravimetric energy density in terms of lightweight and portability of batteries. Moreover, selenium exhibits a quite high intrinsic electronic conductivity (1×10^{-3} S/m) which is about 20 orders of magnitude greater than sulphur [11, 12], indicating better electrochemical activity and better rate capability. Nevertheless, the shuttle effect in Li-Se system that deteriorates the cycle performance due to the dissolution of polyselenide species in electrolytes remains to be a problem [13]. Some strategies used to address the similar issue for Li-S battery can be applied to Li-Se battery, such as, carbon coating [14-16], use of microstructure with various morphology [17, 18], exploration of appropriate electrolyte system [19-21] and other methods of modification [22]. Zhang et al. presented a simple way to improve the specific capacity of Li-Se battery by inserting a conductive, porous carbon interlayer between the cathode and the separator [23]. Wu et al. prepared a Se/C cathode by low temperature treatment which delivered a capacity of 187 mAh/g even at a current density of 500 mA/g [24].

Considering that conductive polymer compounds were repeatedly used in Li secondary batteries due to its good electrochemical activity and better accommodation of volume expansion than carbon [25]. Polypyrrole was

reported to be beneficial to improve the performance of Li-S batteries [26-28] and was also adopted for Se cathode. Kundu et al. [29] studied the performance of nano-fibrous selenium (20-50nm) with polypyrrole coating synthesized by a surfactant free solution method as cathode material and demonstrated that polypyrrole wrapping enhanced the capacity by withstanding the large volume shrinkage and expansion. Considering that polypyrrole is of both electronic and ionic conductivity that can diminish electrochemical polarization, we employed polypyrrole hollow spheres in the cathode for Li-Se battery system in order to confine Se and polyselenides. The loss of active material and capacity fading were effectively suppressed.

Experimental

Synthesis of Se@PPy hollow sphere composite

PPy hollow spheres were synthesized by a modified template process as described in our previous work [30]. The Se@PPy hollow sphere composite was prepared by a melt-diffusion approach. A mixture of Se and PPy hollow spheres (PPy HS) with a 6: 4 weight ratio was mixed uniformly by grinding for 30 minutes. Then the mixture was sealed in an evacuated glass tube and heated at 250 ℃ for 12 h. After that the composite was washed with CS_2 solvent 3 times to remove the unconfined Se.

Physical Characterization

Field emission scanning electron microscope (FESEM) images were obtained by a JSM-6700 field emission scanning electron microscope. Transmission electron microscope analysis was performed on a JEOL JEM-2010 transmission electron microscope (TEM) operated at 200 kV. The elemental mapping results were examined with an energy dispersive spectrometer (EDS) attached to the JEOL JEM-2010 TEM. X-ray powder diffraction (XRD) analysis of the as-obtained samples was carried out with a Rigaku Ultima IV with CuK_α radiation (λ= 1.54056 Å) operated at 40 kV and 200 mA. Raman spectroscopy measurements were conducted by using a DXR Raman Microscope (Thermo Fisher) with an excitation length of 532nm. An elemental analyser (Vario EL III, Elementar Corp.) was applied to determine the content of Se in the composite. The specific surface area was measured using the Brunauer-Emmett-Teller (BET) method on a Micromeritics Tristar 3000.

The cycled Li anode samples for SEM measurements were prepared in the argon-filled glove box. The cells were disassembled after cycling and the cycled Li foils were washed with pure 1, 2-dimethoxyethane (DME, anhydrous, Sigma) and then dried for 2h. A special transfer system[31] was employed to transfer the cycled lithium samples from the glove box to a SEM system without being exposed to air.

Electrochemical Characterization

The electrochemical performance of Se@PPy HS composite was assessed using CR2025 type coin cells assembled in an argon-filled glove box with oxygen and water contents less than 1 ppm. To prepare the cathode, a slurry containing 80 wt% composite material, 10 wt% acetylene black, 5 wt% carboxyl methyl cellulose, 5 wt% styrene-butadiene rubber, dissolved in a proper amount of deionized water, was mixed through ball milling at 250 r/min for 6 h. For comparison, the slurry of pristine selenium was prepared in the same way. After that, the slurries were pasted on an Al foil. The electrodes were dried at 60 °C under vacuum for 12 h after the solvent was evaporated and then were cut into discs with 14 mm in diameter. A solution of 1 M lithium bis(trifluoro-methanesulfonyl)imide (LiTFSI) plus 0.1 M $LiNO_3$ dissolved in 1, 3-dioxolane (DOL) / DME with a volume ratio of 1:1 was employed as the electrolyte. A glass fiber and lithium foil were used as the separator and the anode, respectively.

Galvanostatic discharge/charge tests were performed on a LAND CT2001A battery test system (Wuhan, China) in a voltage range of 1.6 - 2.6 V (vs. Li/Li^+). AC impedance spectroscopy data were collected over a frequency range from 0.01 Hz to 1M Hz with a potential amplitude of 10 mV on an Autolab Electrochemical Workstation (ECO CHEMIE B.V, Netherlands). Cyclic voltammetry (CV) measurement was also conducted on the Autolab Electrochemical Workstation at 0.1 mV/s in the potential range of 1.0 - 3.0 V. All the electrochemical measurements were carried out at room temperature. The value of Coulombic efficiency is determined via dividing the discharge capacity by the charge capacity of each cycle.

Results and Discussion

The morphology of prepared PPy hollow spheres is shown in figure 1a and b. The hollow spheres are self-assembled by smaller polypyrrole particles, with an approximate diameter of 300 nm and present good shape and dispersibility with nice uniformity not only in particle size but also in shell thickness. Figure 1c shows the morphology of Se@PPy HS composite and corresponding C and Se elemental mapping. With a high selenium content of 52.4 wt%, no distinct Se particles or agglomerations were observed around PPy spheres. EDS mapping results of the composite show uniform distribution of Se within spheres or on the outer surface of them, indicating the infiltration of selenium into the hollow spheres. Furthermore, the specific surface area of the composite

dramatically reduces, compared to the one of PPy HS, as seen in figure S1 †, which confirms the penetration of Se into PPy HS.

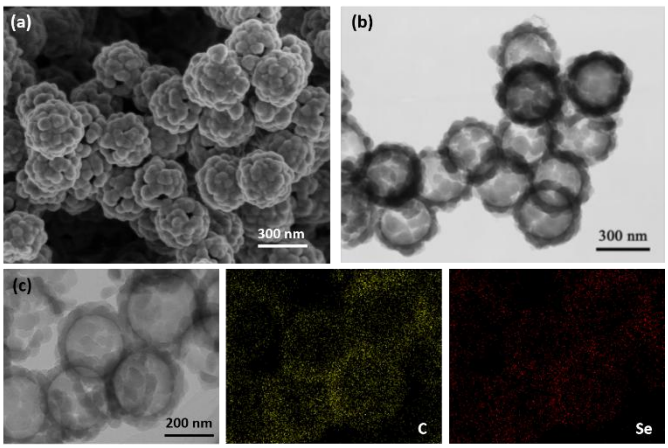

Figure 1. a) SEM image of PPy hollow spheres; b) TEM images of PPy hollow spheres and c) Se@PPy HS and corresponding C and Se elemental mapping.

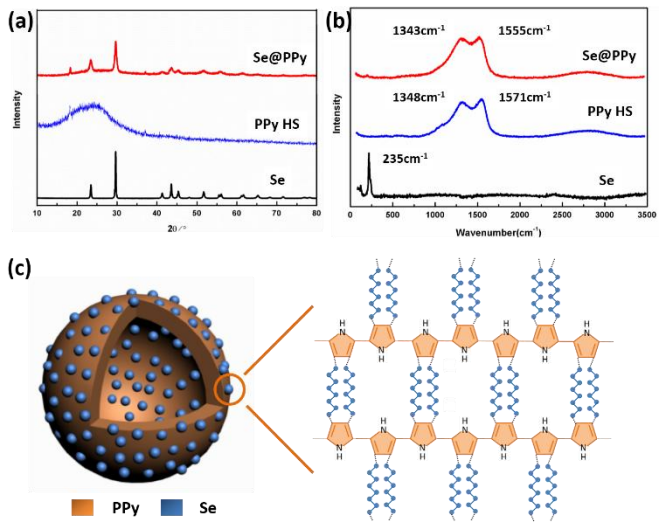

Figure 2. a) XRD patterns of Se, PPy HS and Se@PPy HS; b) Raman spectra of Se, PPy HS and Se@PPy HS; c) schematic illustration of Se@PPy HS composite and a possible spatial structure for it.

Figure 2 shows the XRD patterns of pristine Se, PPy HS and the Se@PPy HS composite. All the diffraction peaks of pristine Se, of extreme sharpness and high intensity, can be indexed as those of the trigonal phase of selenium. By comparison, the identical diffraction peaks of Se in the Se@PPy HS composite become much weaker and broadening, which indicates that part of crystalline Se transforms into amorphous one and most of Se has diffused into the hollow spheres.

The structure feature of Se in the composite was further probed by Raman Spectroscopy (Figure 2b). Compared with the pristine Se, the intensity of characteristic peak of Se highly decreases in Se@PPy HS composite but the spectrum of the composite still shows a small peak at 236 cm^{-1} which is corresponding to the chain-structured Se_n molecule [32], thus indicating the impregnation of Se into the PPy hollow spheres [13]. Chain-like Se_n molecules are likely to exhibit superior electrochemical properties because of the strong interaction with the host matrix [33]. In the spectra of PPy, a major broad band at 1348 cm^{-1} is assigned to a hybrid mode of intra-ring C-C bond stretching and mainly inter-ring C-C bond stretching, antisymmetrical C-N stretching or ring stretching [34]. The other band at 1571 cm^{-1} is assigned to the C=C backbone stretch contributed by the cation species [35]. However, after encapsulation of Se into PPy hollow spheres, the band at 1348 cm^{-1} red shifts to 1343 cm^{-1} while the C=C band shifts to 1555 cm^{-1} which is attributed to neutral species [35]. The shift of bands reveals certain interaction between Se and PPy matrix.

The schematic illustration of the Se@PPy HS composite and a possible spatial structure of it are shown in figure 2c. The thin wall of PPy hollow sphere, which is favorable for both electron conduction and Li ion transport, can physically hinder the dissolution of polyselenides. The volume expansion during cycling can be well buffered by the hollow space. Furthermore, the interaction force between chain-like Se_n and PPy generated during the heat treatment can also play a part in inhibiting the shuttle effect. According to the above Raman analysis, C=C backbone stretch in PPy alters a little after the infiltration of Se. So we can speculate that part of chain-like Se_n in the composite has certain interaction with the C atom in C=C bond as indicated by the black dotted line in figure 2c. Thus a cross-linked Se-PPy network is developed. A similar phenomenon is observed in S@PPy composite [30].

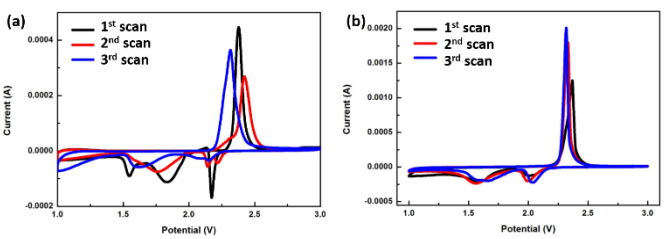

Figure 3. Cyclovoltammetric behavior of pristine Se a) and Se@PPy HS electrode b) performed at a scan rate of 0.1 mV/s between 1.0 and 3.0 V against Li^+/Li.

The CV curves of Li/Se and Li/Se@PPy HS cells are shown in Figure 3. The curves of pristine Se cathode vary a lot with the increase of scanning laps while the ones of Se@PPy HS cathode almost overlap together, thus confirming that the composite cathode displays high reversibility and stability. The cathodic peak current of the composite electrode is 4 times as high as the one of pristine Se, implying higher electrochemical

activity of Se@PPy HS cathode. During the initial discharge process of Li/Se@PPy HS cell, two cathodic peaks at 2.04 V and 1.60 V are noted, corresponding to the conversion of elemental Se to polyselenides and polyselenides to Li_2Se, respectively. Only one anodic peak (Li-extraction) is observed at 2.37 V in the subsequent anodic sweeping to 3.0 V. In the second and third cycles, the reduction peaks shift by 0.03 V to a higher potential while the oxidation ones shift to a lower potential by 0.04 V. The slight shift in the peak potentials indicates a decrease in electrochemical polarization and good reversibility of Se@PPy HS composite. Furthermore, the oxidation peak current becomes greater as the scanning continues, which is related to the activation of electrochemical process.

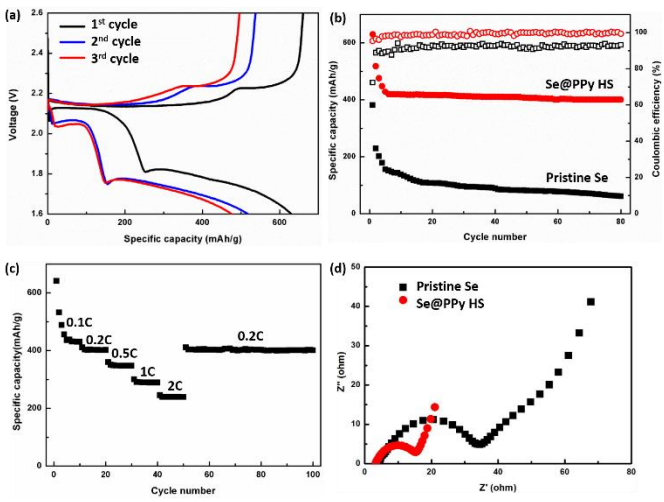

Figure 4. a) Glavanostatic discharge/charge voltage profiles of Se@PPy HS at 0.2C; b) Cycling performance and Coulombic efficiency of Se@PPy HS and pristine Se at 0.2C; c) rate capability of Se@PPy HS cathode; d) Nyquist plots of Li- Se@PPy HS and Li-Se cell after 50 cycles.

Figure 4a displays the Glavanostatic discharge/charge voltage profiles of the Se@PPy HS cathode at 0.2C between 1.6 V and 2.6 V. Consistent with the cyclic voltammetry curves, two discharge plateaus are shown in the discharge curves, which can be attributed to the two classical step reactions of elemental selenium with lithium during the discharge process [36]. The composite cathode delivers an initial discharge capacity of 630mAh/g. Figure 4b compares the specific discharge capacity and Coulombic efficiency of Se@PPy HS and pristine Se at 0.2 C rate. Pristine Se cathode presents rather poor cycling stability with a low reversible capacity of less than 45 mAh/g after 80 cycles. The severe capacity fading is ascribed to the shuttle effect with dissolution of polyselenide species generated during discharging process which also results in lower coulombic efficiency. By contrast, a specific discharge capacity of 400 mAh/g is obtained for Se@PPy HS electrode after 80 cycles. Moreover, the Coulombic efficiency almost reaches 100%, indicating that the shuttle effect are effectively inhibited by the hollow structure of the PPy matrix (The Coulombic efficiency displayed in a smaller scale range is shown in figure S2 †). The large capacity loss during the first five cycles can be interpreted as follows. A part of Se in the composite cathode is free and dissociative instead of being restricted inside the hollow spheres or connected with PPy. The polyselenide species generated by these dissociative Se during the discharge process dissolve in the electrolyte and migrate to the anode, thus resulting in the loss of active mass. It's the other part of Se inside the hollow spheres or interacted with PPy that contributes to the stable discharge capacity in subsequent cycles.

The Se@PPy HS cathode also shows excellent rate capability (figure 4c). The discharge capacity gradually decreases as the current rate increases from 0.1 C to 2 C (1 C is 675 mAh/g). Capacity of 238 mAh/g is still retained at 2 C and it recovers to 402 mAh/g when the current rate is back to 0.1 C, indicating the high reversibility of the composite cathode. Even after 100 cycles, capacity of 399 mAh/g is retained. The good rate capability of the composite cathode can be attributed to the facile electronic/ionic transport and high reaction kinetics in the Se@PPy HS.

Electrochemical impedance spectroscopy (EIS) provides further evidence for the superior cyclability of Se@PPy HS composite as figure 4d indicates. The data show that the charge transfer resistance (R_{ct}) obviously reduces when pristine Se is substituted by Se@PPy HS as cathode, demonstrating higher electrochemical activity of the composite cathode. The improved electrochemical activity can be ascribed to less corrosion of the Li surface, which results from the suppression of shuttle effect during cycling.

After 50 cycles, two kinds of cells were disassembled. The Li anodes were observed by photograph on the macroscopic scale as shown in the insets of figure 6. The displayed Li surface is the side close to the separator. It can be clearly seen that the Li anode from Li/Se cell appears partially black and dark on the surface, indicating the severe corrosion by the reaction with polyselenides. On the contrary, the cycled Li anode from Li/Se@PPy HS cell presents metallic luster with little distinction from the fresh micro perspective. The Li anode from Li/Se cell shows uneven and coarse morphology (figure 6a) while a smooth and flat surface is shown in figure 6b, demonstrating that only a little polyselenides migrate from the Se@PPy HS cathode to the anode side and thus shuttle effect is greatly restrained.

The SEM images of cycled Li cross-section provide another strong evidence for the shuttle effect suppression of Se@PPy HS cathode. The corrosion of Li anode by

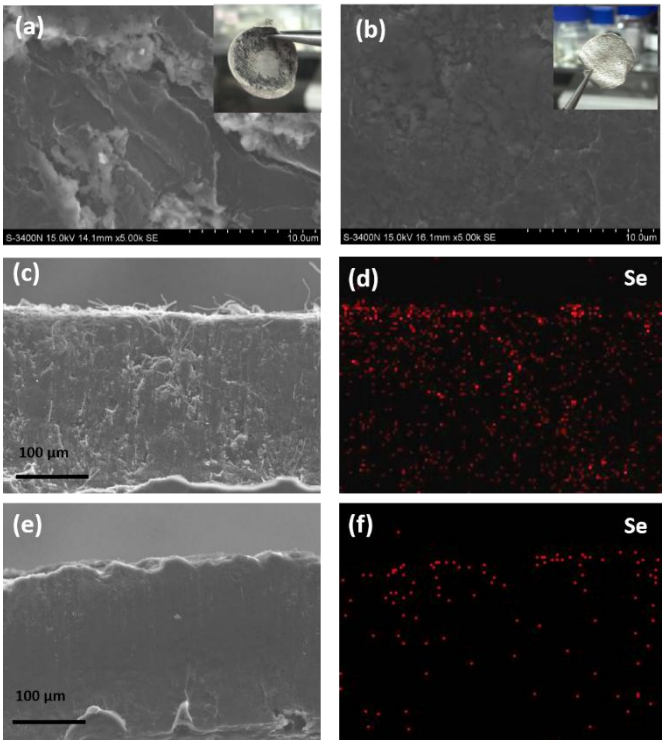

Figure 6. SEM images of Li surface disassembled from Li-pristine Se cell (a) and Li-Se@PPy HS cell (b) after 50 cycles at 0.1 C. (inset: pictures of corresponding Li anode). SEM images and corresponding Se elemental mapping of Li cross-section disassembled from Li-pristine Se cell (c, d) and Li-Se@PPy HS cell (e, f) after 50 cycles at 0.1 C.

polyselenides in Li/Se cell is so severe that both the upper surface and the internal mass are eroded as presented in figure 6c and d. By comparison, the cross-section of Li in cycled Li/Se@PPy HS cell shows a little bit corrosion (figure 6e, f). These results convincingly prove that Se@PPy HS cathode successfully inhibits the shuttle effect and improves the electrochemical performance of Li-Se battery by accommodating the soluble polyselenides into the hollow spheres and adsorbing them via certain interaction by PPy.

Conclusions

In summary, Se@PPy HS composite that delivers a specific discharge capacity of 400 mAh/g after 80 cycles and a coulombic efficiency of nearly 100%, can be considered as a favorable cathode in Li-Se battery system. Since the hollow sphere structure plays an effective role in accommodating and confining soluble intermediate discharge products, shuttle effect that brings about severe capacity fading and poor cycle performance is greatly suppressed.

Acknowledgements

The authors highly acknowledge Prof. B. V. R. Chowdari (National University of Singapore) for his helpful discussions and the Natural Science Foundation of China for its financial support (NSFC, Projects No. 51402330 and No. 51201177).

Notes and references

[a] CAS Key Laboratory of Materials for Energy Conversion, Shanghai Institute of Ceramics, Chinese Academy of Sciences, Shanghai 200050, P. R. China. Fax: +86-21-52413903; Tel: +86-21-52411704; E-mail: zywen@mail.sic.ac.cn

† Electronic Supplementary Information (ESI) available. See DOI: 10.1039/c000000x/

1. M. Wakihara, *Mat Sci Eng R*, 2001, **33**, 109-134.
2. J. Vetter, P. Novak, M. R. Wagner, C. Veit, K. C. Moller, J. O. Besenhard, M. Winter, M. Wohlfahrt-Mehrens, C. Vogler and A. Hammouche, *Journal of Power Sources*, 2005, **147**, 269-281.
3. X. L. Ji and L. F. Nazar, *Journal of Materials Chemistry*, 2010, **20**, 9821-9826.
4. A. Manthiram, Y. Z. Fu and Y. S. Su, *Accounts Chem Res*, 2013, **46**, 1125-1134.
5. J. R. Akridge, Y. V. Mikhaylik and N. White, *Solid State Ionics*, 2004, **175**, 243-245.
6. P. G. Bruce, S. A. Freunberger, L. J. Hardwick and J. M. Tarascon, *Nat Mater*, 2012, **11**, 19-29.
7. Z. L. Wang, D. Xu, J. J. Xu, L. L. Zhang and X. B. Zhang, *Adv Funct Mater*, 2012, **22**, 3699-3705.
8. R. Black, B. Adams and L. F. Nazar, *Adv Energy Mater*, 2012, **2**, 801-815.
9. Z. Q. Peng, S. A. Freunberger, Y. H. Chen and P. G. Bruce, *Science*, 2012, **337**, 563-566.
10. R. Padbury and X. W. Zhang, *Journal of Power Sources*, 2011, **196**, 4436-4444.
11. A. Abouimrane, D. Dambournet, K. W. Chapman, P. J. Chupas, W. Weng and K. Amine, *Journal of the American Chemical Society*, 2012, **134**, 4505-4508.
12. L. Liu and Y. Wu, *Chem.Commun.*, 2013, **49**, 11515-11517.
13. C. P. Yang, S. Xin, Y. X. Yin, H. Ye, J. Zhang and Y. G. Guo, *Angew Chem Int Edit*, 2013, **52**, 8363-8367.
14. X. Liang, Z. Y. Wen, Y. Liu, H. Zhang, J. Jin, M. F. Wu and X. W. Wu, *Journal of Power Sources*, 2012, **206**, 409-413.
15. M. Q. Zhao, X. F. Liu, Q. Zhang, G. L. Tian, J. Q. Huang, W. C. Zhu and F. Wei, *Acs Nano*, 2012, **6**, 10759-10769.
16. F. Wu, J. Z. Chen, L. Li, T. Zhao and R. J. Chen, *J Phys Chem C*, 2011, **115**, 24411-24417.
17. J. Y. Li, B. Ding, G. Y. Xu, L. R. Hou, X. G. Zhang and C. Z. Yuan, *Nanoscale*, 2013, **5**, 5743-5746.
18. X. A. Liang, Z. Y. Wen, Y. Liu, H. Zhang, L. Z. Huang and J. Jin, *Journal of Power Sources*, 2011, **196**, 3655-3658.
19. S. S. Jeong, Y. T. Lim, B. S. Jung and K. W. Kim, *Mater Sci Forum*, 2005, **486-487**, 594-597.

20. S. S. Zhang, *Electrochimica Acta*, 2013, **97**, 226-230.
21. S. Z. Xiong, K. Xie and X. B. Hong, *Chem J Chinese U*, 2011, **32**, 2645-2649.
22. J. Q. Huang, Q. Zhang, S. M. Zhang, X. F. Liu, W. C. Zhu, W. Z. Qian and F. Wei, *Carbon*, 2013, **58**, 99-106.
23. Z. Zhang, Z. Zhang, K. Zhang, X. Yang and Q. Li, *RSC Advances*, 2014, **4**, 15489.
24. L. Liu, Y. Hou, Y. Yang, M. Li, X. Wang and Y. Wu, *RSC Advances*, 2014, **4**, 9086.
25. Y. Yang, G. Zheng and Y. Cui, *Chemical Society reviews*, 2013, **42**, 3018-3032.
26. Y. Fu and A. Manthiram, *Rsc Advances*, 2012, **2**, 5927-5929.
27. Y. Zhang, Y. Zhao, D. The Nam Long, A. Konarov, D. Gosselink, H. G. Soboleski and P. Chen, *Solid State Ionics*, 2013, **238**, 30-35.
28. Y. Zhang, Y. Zhao, A. Konarov, D. Gosselink, Z. Li, M. Ghaznavi and P. Chen, *Journal of Nanoparticle Research*, 2013, **15**, 1-7.
29. D. Kundu, F. Krumeich and R. Nesper, *Journal of Power Sources*, 2013, **236**, 112-117.
30. G. Ma, Z. Wen, J. Jin, Y. Lu, X. Wu, C. Liu and C. Chen, *RSC Advances*, 2014, **4**, 21612.
31. S. Xiong, K. Xie, Y. Diao and X. Hong, *Electrochimica Acta*, 2012, **83**, 78-86.
32. C. Luo, Y. H. Xu, Y. J. Zhu, Y. H. Liu, S. Y. Zheng, Y. Liu, A. Langrock and C. S. Wang, *Acs Nano*, 2013, **7**, 8003-8010.
33. H. Ye, Y.-X. Yin, S.-F. Zhang and Y.-G. Guo, *J Mater Chem A*, 2014, **2**, 13293-13298.
34. V. Eshkenazi, E. Peled, L. Burstein and D. Golodnitsky, *Solid State Ionics*, 2004, **170**, 83-91.
35. K. Crowley and J. Cassidy, *Journal of Electroanalytical Chemistry*, 2003, **547**, 75-82.
36. Y. Cui, A. Abouimrane, J. Lu, T. Bolin, Y. Ren, W. Weng, C. Sun, V. A. Maroni, S. M. Heald and K. Amine, *Journal of the American Chemical Society*, 2013, **135**, 8047-8056.